ISSN: 2996-2498

Research Article

Environmental Science and Climate Research

Multiscale Relationships Between ENSO and Tropical Cyclones Over the Western North Pacific (1950–2024) An Empirical Study Based on Wavelet Analysis

Chang Xiaoli[1], Xiang Canke[1*], Qiu Jingjia[2], Cao Yu[1], Ouyang Wenqi[1], Huang Mei[1], Du Yifei[1] and Chen Shuyang[1]

[1]*School of Earth Sciences and Spatial Information Engineering, Hunan University of Science and Technology, Xiangtan 411201, Hunan, China*

[2]*School of Architecture and Design, Hunan University of Science and Technology, Xiangtan 411201, Hunan, China*

[*]Corresponding Author
Xiang Canke, School of Earth Sciences and Spatial Information Engineering, Hunan University of Science and Technology, Xiangtan 411201, Hunan, China.

Submitted: 2026, Feb 16; **Accepted:** 2026, Mar 12; **Published:** 2026, Mar 31

Citation: Xiaoli, C., Canke, X., Jingjia, Q., Yu, C., Wenqi, O., et al. (2026). Multiscale Relationships Between ENSO and Tropical Cyclones Over the Western North Pacific (1950–2024) An Empirical Study Based on Wavelet Analysis. *Env Sci Climate Res, 4*(1), 01-16.

Abstract

Based on tropical cyclone data from the China Meteorological Administration and the Oceanic Niño Index data, this study statistically analyzed the intensity changes of ENSO events and characteristics such as the frequency and intensity of typhoons in the Northwest Pacific over the past nearly 75 years (1950-2024). Wavelet analysis was employed to examine the time-frequency characteristics of ENSO and its correlation with Northwest Pacific tropical cyclons (referred to as typhoons in the Northwest Pacific). The results indicate that: 1) ENSO exhibits an interannual oscillation with a timescale of 94 months (approximately 5-year cycle) and an interdecadal oscillation with a timescale of 198 months (approximately 10-11 year cycle). 2) Over the past 75 years, the frequency of Northwest Pacific typhoons and landfalling typhoons has significantly decreased, while the landfall intensity has significantly increased; typhoon frequency is highest in August and lowest in February, while typhoon intensity is strongest in October and weakest in February. 3) On the interannual scale, there is a negative correlation between ENSO and typhoon frequency, as well as landfalling typhoon frequency, at the 2-6 year timescale, with moderate significance, and typhoon changes slightly lead ENSO; there is a positive correlation between ENSO and average typhoon intensity, as well as average landfalling typhoon intensity, at the 2-6 year and 10-15 year timescales, with strong significance, and ENSO changes slightly lead typhoon changes. 4) On the monthly scale, the negative correlation between ENSO and typhoon frequency is more significant than on the interannual scale, whereas the positive correlation between ENSO and average typhoon intensity is less significant than on the interannual scale. Furthermore, the positive/negative correlation between ENSO and typhoon frequency shows different directions depending on the chosen cycle scale.

Keywords: ENSO, Western North Pacific Tropical Cyclones, Oceanic Niño Index (ONI), Frequency, Intensity, Wavelet Analysis

1. Introduction

A tropical cyclone (TC) is an intense cyclonic vortex with a warm-core structure that forms over tropical oceans [1]. It is referred to as a "typhoon" in the Northwest Pacific and its coastal areas. Typhoons often bring extreme weather such as strong winds, heavy rainfall, and storm surges, possessing significant destructive power [2,3]. Northwest Pacific typhoons refer to those occurring in the Northwest Pacific, north of the equator, west of the dateline, affecting Asian Pacific countries or regions. The Northwest Pacific, being the most active typhoon genesis region globally (accounting for 38% of the global total number of TCs), has the highest frequency and intensity of typhoons in the world [4]. China, located on the western coast of the Northwest Pacific, is one of the countries most severely affected by typhoons globally, suffering substantial economic losses and casualties annually due to typhoons, especially in coastal regions

like Guangdong and Zhejiang [5,6]. In 2021, the strong Typhoon "In-Fa" made landfall in Zhejiang, subsequently forming a dual-typhoon water vapor transport system with Typhoon "Cempaka", causing extreme rainfall in Henan with a daily precipitation of 663.9 mm and a maximum hourly precipitation of 201.9 mm. Zhengzhou, the precipitation center, experienced extremely severe urban flooding [7,8]. In 2023, the super typhoon "Doksuri" made landfall in Fujian, and its remnant circulation moved northward deep inland, causing persistent extreme rainfall in North China and the Huang-Huai region, with maximum rainfall reaching 1003.4 mm, triggering mountain floods in Beijing, Hebei, and other areas [9,10]. Therefore, revealing the multiscale variability of Northwest Pacific typhoon activity and its coupling mechanism with ENSO holds significant scientific importance for improving seasonal typhoon prediction models. Multidisciplinary studies have confirmed that ENSO (El Niño-Southern Oscillation), as the dominant mode of interannual climate variability, is essentially a self-sustained oscillation of the tropical Pacific ocean-air coupling system, which manifests itself in the ocean as an abnormally high sea temperature in the eastern Pacific Ocean (ENSO warm phase) [11]. Abnormal cooling produces La Niña phenomenon (ENSO cold phase) [12,13]. The ENSO cycle significantly affects the global climate system by altering the atmospheric circulation of the tropical Pacific, especially modulating the location and intensity of typhoons. In 1999, a strong La Niña event lasted for three years, and the intensity of typhoons in the northwest Pacific reached a record low, while in 2016, a super El Niño event occured, and the intensity of typhoons in the northwest Pacific reached a record high, with ENSO having a certain effect on typhoon intensity [14,15]. In 2023, the three-year La Niña state quickly subsided and turned sharply into El Niño, followed by a strong El Niño event, with only 15 typhoons in the northwest Pacific that year, the second lowest in history since 1950, but their average intensity far exceeded the historical average, reaching typhoon level and ranked sixth on average intensity in history, among them 8 were super typhoons, exceeding 50%, reaching one of the highest super typhoon rates recorded in history. The correlation between super typhoons and ENSO was particularly obvious [16,17]. It can be seen that the frequency and intensity of typhoons in the northwest Pacific are inseparable from the ENSO cycle.

Extensive research has been conducted in the past regarding the correlation between ENSO and the frequency and intensity of typhoons. Huang Yong et al. proposed that the number of typhoons generated in the Northwest Pacific is relatively lower during El Niño years [18,19]. Mao Lanhua et al. pointed out that the frequency of typhoons making landfall in China during El Niño years is also lower than in La Niña years [20,21]. Ji Qianqian noted that a negative phase resonance cycle exists between ENSO and the frequency of typhoons in the South China Sea [22]. The above studies all involve conclusions regarding a negative correlation between ENSO and typhoon frequency, yet research on the correlation with typhoon intensity remains insufficient. Subsequently, Yu Qiqian proposed that ENSO is significantly positively correlated with the average intensity of typhoons affecting the Chinese coast [23]. Li Zheng pointed out that ENSO is significantly positively correlated with the lifetime intensity of northward-moving typhoons [24]. It can be seen that past studies consistently suggest that El Niño can, to a certain extent, suppress typhoon frequency and enhance typhoon intensity. However, limitations persist, such as singular research parameters, incomplete research objects, insufficient time spans, or incomplete spatial scopes, making it difficult to fully characterize the dynamic coupling mechanism between ENSO and the frequency and intensity of typhoons in the Northwest Pacific. This study integrates long-term typhoon observation data from the past 75 years with ENSO indices, with the spatial scope of typhoon data covering the entire Northwest Pacific. By applying wavelet analysis, this research achieves multi-scale dynamic decoupling between ENSO and a multi-parameter typhoon system (frequency, intensity, landfall frequency, and landfall intensity) in the time-frequency domain, breaking through the limitations of previous research in terms of objects and spatio-temporal scope.

2. Data and Methodology

2.1. Ocean Nino Index Data

We adopted the Oceanic Niño Index (ONI) provided by the National Oceanic and Atmospheric Administration/Climate Prediction Center (NOAA/CPC) (https://origin.cpc.ncep.noaa.gov/products/) to characterize the intensity of ENSO events. The ONI is derived from the 3-month running average of Sea Surface Temperature Anomalies (SSTA) in the Niño 3.4 region (5°N–5°S, 170°–120°W).

It is stipulated that an El Niño or La Niña event is identified when the absolute value of the 3-month running average for Niño 3.4 reaches or exceeds 0.5°C for at least five consecutive months; specifically, an ONI ≥ 0.5°C constitutes an El Niño event, while an ONI ≤ -0.5°C constitutes a La Niña event [25,26].

2.2. Tropical Cyclone Data and Typhoon Classification Standards

The tropical cyclone data used in this paper are sourced from the "CMA Best Track Dataset" and the "Landing Tropical Cyclone Dataset" provided by the Tropical Cyclone Data Center of the China Meteorological Administration (tcdata.typhoon.org.cn). This dataset has undergone multi-source observational data assimilation and retrospective correction; the data selected for this study were last updated on April 2, 2025. The current version of the CMA Best Track Dataset provides the position and intensity information of tropical cyclones in the Northwest Pacific (including the South China Sea, north of the equator and west of 180°E) every 6 hours since 1949. Landing tropical cyclones refer to those that make landfall in China; coastal islands, with the exception of Taiwan, the Zhoushan Archipelago, Hong Kong, Hainan Island, and Chongming Island, are not treated as landfall locations [27,28]. Considering that the Oceanic Niño Index records began in 1950, the period of typhoon coverage in this paper starts from 1950.

According to the National Standard for "Grade of Tropical Cyclones" (GB/T 19201–2006), the intensity of tropical cyclones is divided into six grades, which from weakest to strongest are:

Tropical Depression (TD), Tropical Storm (TS), Severe Tropical Storm (STS), Typhoon (TY), Severe Typhoon (STY), and Super Typhoon (Super TY) [29]. In this paper, numerical values are assigned to the extreme intensity levels of typhoons based on this standard to facilitate the statistics of typhoon intensity changes, as shown in Table 1:

Typhoon IIntensity	Intensity Assignment	Description
Tropical depression	1	Wind speed 10.8–17.1m/s, wind force 6–7
Tropical storm	2	Wind speed 17.2–24.4 m/s, wind force 8–9
Severe tropical storm	3	Wind speed 24.5–32.6 m/s, wind force 10–11
typhoon	4	Wind speed 32.7–41.4 m/s, wind force 12–13
Strong typhoon	5	Wind speed 41.5–50.9 m/s, wind force 14–15
Super typhoon	6	wind speed ≥ 51.0 m/s, wind force ≥ level 16

Table 1: Typhoon Intensity Levels and their Assignments

2.3. Research Methodology

In this paper, wavelet analysis is used to analyze the time-frequency characteristics of ENSO and its time-frequency resonance law with typhoon parameters, and reveal the phase relationship between the two.

First, the Continuous Wavelet Transform (CWT) is introduced. For a given time series x(t), the continuous wavelet transform can be expressed as:

$$W_x(\tau,s) = \int_{-\infty}^{\infty} x(t)\psi^*_{\tau,s}(t)dt \quad (1)$$

wherein represents the subwavelet family obtained by the parent wavelet base function as the scale expansion and time translation:

$$\Psi_{\tau,s}(t) = \frac{1}{\sqrt{s}}\psi\left(\frac{t-\tau}{s}\right), s,\tau \in \mathbb{R}, s \neq 0 \quad (2)$$

where and s are translation and scale factors, respectively. The position of the wavelet in the time domain is determined by the former and by the latter in the frequency. The Morlet wavelet is selected as the parent wavelet function, and its form can simultaneously optimize the time-frequency resolution (see Equation 3) to meet the needs of non-stationary signal analysis, which is defined as follows:

$$\psi(t) = \pi^{-\frac{1}{4}} e^{iw_0 t} e^{-\frac{t^2}{2}} \quad (3)$$

Through continuous wavelet transformation, we can obtain information about time series in the time and frequency domains. We perform continuous wavelet transformation of signals of different frequencies to obtain time-frequency graphs. From the diagram, we can intuitively discover the frequency characteristics of the signal.

The application of continuous wavelet transform is mainly focused on multi-scale analysis of single variables, but in order to be able to analyze the correlation between two variable sequences in both the time-frequency domain at the same time, cross wavelet transform (XWT) is used. Given the time series x(t) and y(t), the cross-wavelet transform can be expressed as:

$$w_{xy}(\tau,s) = w_x(\tau,s)w^*_y(\tau,s) \quad (4)$$

Wx and Wy represent the continuous wavelet transformations of the time series x(t) and y(t), respectively. It reflects the local covariance of two variables over a specific time-frequency domain. To measure the coherence of two variables in the time-frequency domain, wavelet coherence (WTC) is introduced, which is defined as:

$$R^2(\tau,s) = \frac{\left|S\left(s^{-1}W_{xy}(\tau,s)\right)\right|^2}{S(s^{-1}|W_x(\tau,s)|)S(s^{-1}|W_y(\tau,s)|)} \quad (5)$$

where S represents the smoothing operator. Wavelet coherence can be seen as a local correlation between markets in the frequency domain. Its value range is between 0 and 1, and a high (low) value indicates a strong (weak) correlation between variables.

Wavelet coherence is a square term that cannot determine the lag relationship between markets. Wavelet phase difference can be used to describe the leading lag relationship between the scale components of two time series. For time series $x(t)$, $y(t)$, phase difference is defined as:

$$\phi_{xy} = tan^{-1}\left(\frac{I(W_{xy}(\tau,s))}{R(W_{xy}(\tau,s))}\right), \phi_{xy} \in [-\pi,\pi] \quad (6)$$

where I and R represent imaginary and real operators, respectively. If the phase difference is 0, it means that the two time series fluctuate in the same direction; If the value range of the phase difference is (0, π/2) or (−π, −π/2),$x(t)$ ahead of $y(t)$;If the value range of the phase difference is (π/2, π) or (−π/2,0), $y(t)$ ahead of $x(t)$; If the difference in phase is π(−π), it shows that the two time series fluctuate in the opposite direction in a specific time-frequency space. Through wavelet coherence and phase difference,

we can not only know the strength of the correlation between two time series at different times and scales, but also know the leading lag relationship between variables.

3. ENSO Time-Frequency Characteristic Analysis

3.1. Statistics and Intensity Changes of ENSO Events

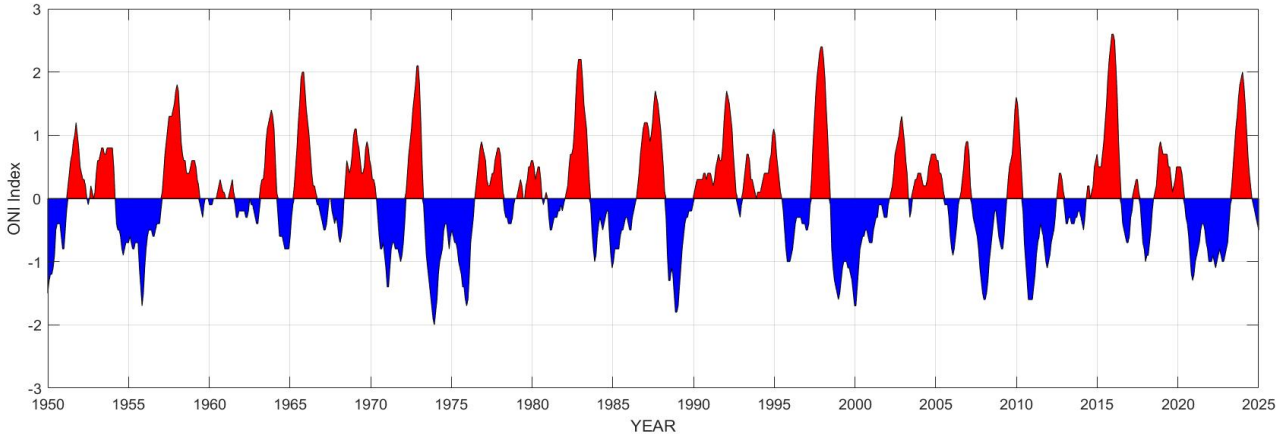

Figure 1: ONI Time Series from 1950 to 2024 (Warm for El Niño, cool for La Niña)

The ocean Niño index ONI is a 3-month sliding average of the sea surface temperature anomaly in the Niño 3.4 sea area. Based on ONI data, we plotted the ONI time series from January 1950 to December 2024, as shown in Figure 1, with the red part representing the El Niño state and the blue part indicating the La Niña state. According to statistics, there were 24 El Niño events and 20 La Niña events between 1950 and 2024, indicating that El Niño events occur more frequently than La Niña events.

In recent years, the National Oceanic and Atmospheric Administration (NOAA) and the China Meteorological Administration (CMA) have used the ocean Nino index ONI to define the intensity of ENSO events:0≤|ONI|≤0.5 neuter, 0.6≤ |ONI|≤0.9 weak, 1≤|ONI|≤1.4 Medium, 1.5≤|ONI|≤1.9 strong, 2≤|ONI| very strong [30-32]. Based on the above intensity definitions, this paper summarizes the intensity levels of all ENSO events and produces a statistical table of El Niño/La Niña events from 1950 to 2024, as shown in Table 2.

El Niño					La Niña				
number	**Start and end time**	**Duration/ month**	**Peak intensity/°C**	**Strength grade**	**number**	**Start and end time**	**Duration/ month**	**Peak intensity/°C**	**Strength grade**
1	1951.06—1952.01	8	1.2	Medium	1	1950.01—1950.07	7	-1.5	Strong
2	1953.02—1954.02	13	0.8	Weak	2	1954.05—1956.09	29	-1.7	Strong
3	1957.04—1958.07	16	1.8	Strong	3	1964.05—1965.01	9	-0.8	Weak
4	1958.11—1959.03	5	0.6	Weak	4	1970.07—1972.01	19	-1.4	Medium
5	1963.06—1964.02	9	1.4	Medium	5	1973.05—1974.07	15	-2	Very Strong
6	1965.05—1966.04	12	2	Very Strong	6	1974.10—1976.04	19	-1.7	Strong
7	1968.10—1969.05	8	1.1	Medium	7	1983.09—1984.01	5	-1	Medium
8	1969.08—1970.01	6	0.9	Weak	8	1984.10—1985.08	11	-1.1	Medium
9	1972.05—1973.03	11	2.1	Very Strong	9	1988.05—1989.05	13	-1.8	Strong
10	1976.09—1977.02	6	0.9	Weak	10	1995.08—1996.03	8	-1	Medium
11	1977.09—1978.01	5	0.8	Weak	11	1998.07—2001.02	32	-1.7	Strong
12	1979.10—1980.02	5	0.6	Weak	12	2005.11—2006.03	5	-0.9	Weak
13	1982.04—1983.06	15	2.2	Very Strong	13	2007.06—2008.06	13	-1.6	Strong
14	1986.09—1988.02	18	1.7	Strong	14	2008.11—2009.03	5	-0.8	Weak

15	1991.05—1992.06	14	1.7	Strong	15	2010.06—2011.05	12	-1.6	Strong
16	1994.09—1995.03	7	1.1	Medium	16	2011.07—2012.04	10	-1.1	Medium
17	1997.05—1998.05	13	2.4	Very Strong	17	2016.08—2016.12	5	-0.7	Weak
18	2002.06—2003.02	9	1.3	Medium	18	2017.10—2018.04	7	-1	Medium
19	2004.07—2005.02	8	0.7	Weak	19	2020.08—2021.05	10	-1.3	Medium
20	2006.09—2007.01	5	0.9	Weak	20	2021.08—2023.01	18	-1.1	Medium
21	2009.07—2010.03	9	1.6	Strong					
22	2014.10—2016.04	19	2.6	Very Strong					
23	2018.09—2019.06	10	0.9	Weak					
24	2023.05—2024.04	12	2	Very Strong					

Table 2: El Niño/La Niña Event Statistics from 1950 to 2024

According to calculations, the average duration of El Niño events is approximately 10-11 months, while the average duration of La Niña events is approximately 12-13 months; it can be seen that when La Niña events occur, their duration is longer compared to El Niño events. However, the average peak intensity of El Niño events is 1.39°C, and the absolute value of the average peak intensity of La Niña events is 1.29°C; it can be seen that when El Niño events occur, their absolute peak intensity is higher compared to La Niña events. Furthermore, El Niño is more likely to develop into "super" level events, and the frequency and intensity of its super events are higher than those of La Niña, which is inextricably linked to the climate background of superimposed global warming [33].

We conducted a Pearson correlation analysis between the duration and peak intensity of El Niño/La Niña events and found a significant positive correlation between the two. In El Niño and La Niña events, the correlation coefficients between duration and peak intensity are +0.79 and +0.68, respectively. From this, we infer that the longer the duration of El Niño/La Niña, the higher its peak intensity.

3.2. Time and Frequency Characteristics

Climate change involves multiple time scales, manifesting as local variations in different time scale structures in the time domain, and as periodic oscillations at different significance levels in the frequency domain [34]. Continuous Wavelet Transform (CWT) provides a key method for analyzing the time-frequency evolution characteristics of ENSO events by performing multi-scale decomposition of the energy distribution of one-dimensional non-stationary signals. This paper adopts the Morlet wavelet function as the wavelet base function to decompose the ONI index into time-varying energy spectra at different time scales, revealing the multi-scale oscillatory characteristics of ENSO intensity and phase. Furthermore, the CWT results, through significance testing (Red Noise confidence test), can distinguish the real cycles of ENSO signals from random fluctuations. This provides a physical basis for the screening of coupled frequency bands between ENSO and typhoon parameters in subsequent Cross Wavelet and Wavelet Coherence analyses.

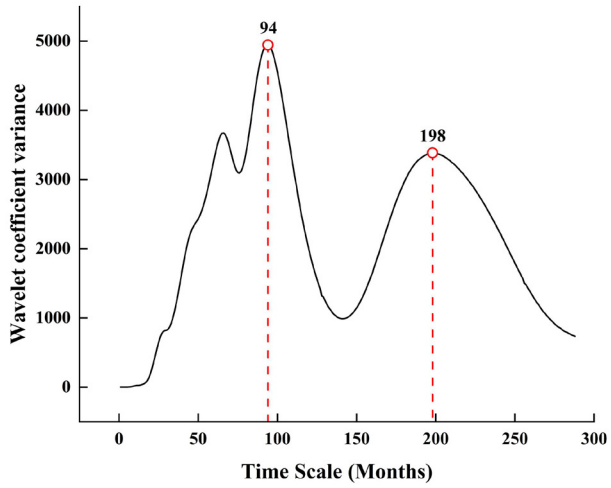

(a)Wavelet coefficient variance plot

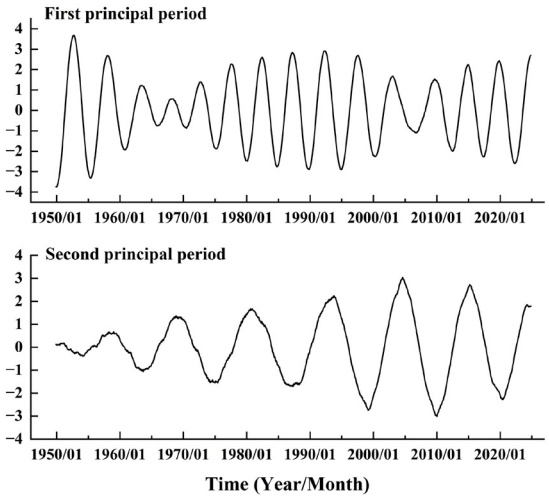

(b) The main period trend chart of the real part of the wavelet coefficient

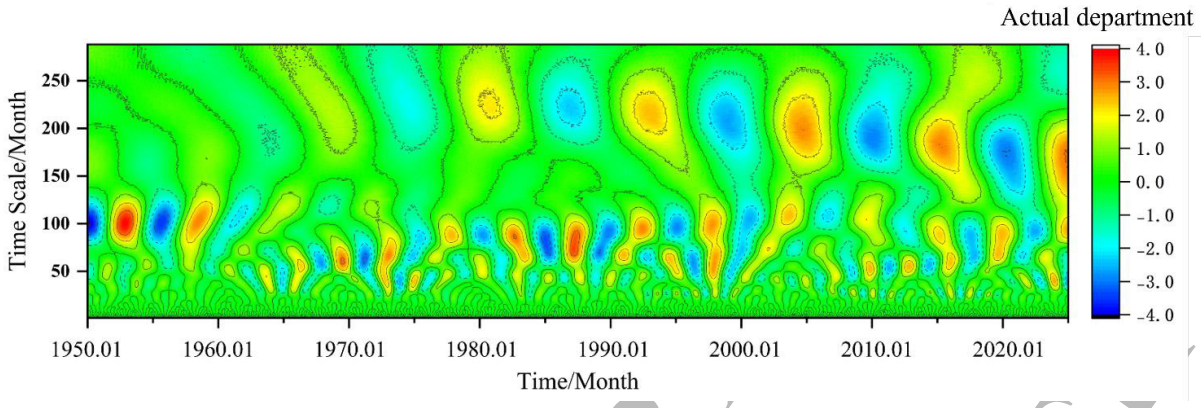

(c) Contour diagram of the real part of the wavelet coefficient

Figure 2: Continuous Wavelet Transform (CWT) of the ONI Index from 1950 to 2024

Figure 2 shows the Continuous Wavelet Transform (CWT) of the ONI index from 1950 to 2024. Figure 2(a) is the wavelet coefficient variance plot, where the x-axis represents the time scale in months and the y-axis represents the wavelet coefficient variance. Figure (b) is the trend plot of the real part of the wavelet coefficients for the primary periods, where the x-axis is time in months and the y-axis is the real part of the wavelet coefficients. Figure (c) is the contour map of the real part of the wavelet coefficients, where the x-axis is time (months), the y-axis is the time scale (months), and positive ONI regions (warm colors) correspond to El Niño states while negative regions (cool colors) correspond to La Niña states.

Each peak's x-coordinate in the wavelet coefficient variance plot represents a primary period—the time scale at which the fluctuation phenomenon occurs—corresponding to the time scale on the y-axis of the contour map. In the wavelet coefficient variance plot (Fig. 2a), there are two significant peaks: the first peak is at 94 and the second is at 198. Correspondingly, in the contour map (Fig. 2c), two primary periods exist in the time scale: the first primary period has a scale of 94 months (7.83 years, approx. 7–8 years), and the second has a scale of 198 months (16.5 years, approx. 16–17 years). This indicates that from 1950 to 2024, the ONI index exhibits a first primary period at a 94-month scale (7–8 years) and a second primary period at a 198-month scale (16–17 years), corresponding to the interannual and decadal oscillations of ENSO, respectively.

In the trend plot of the real part of the wavelet coefficients, the time interval between two peaks represents a period—the repetition interval of the fluctuation phenomenon. In the contour map, this reflects the time interval for a set of signals to complete one positive-negative phase oscillation. In Figure 2(b), the average period of the real part of the wavelet coefficients for the first primary period is 60 months (approx. 5 years), and for the second primary period, it is approximately 10–11 years. This shows that from 1950 to 2024, the ONI index possesses a "small" cycle of about 5 years and a "large" cycle of 10–11 years, corresponding to the 5-year interannual oscillation and the 10–11 years decadal oscillation of ENSO.

Observing the contour map of the real part of the wavelet coefficients reveals that the interannual oscillation of ENSO has three significant periods: the early 1950s to early 1960s, the late 1960s to the early 21st century, and the mid-2010s to the present. During these three periods, the ENSO signal is more prominent with larger amplitudes and higher intensity, while it remains weaker in other periods. The decadal oscillation of ENSO was not significant from the 1950s to the 1980s, with small amplitudes and energy spectrum density below the red noise test threshold ($p>0.1$). However, starting from the 1980s, the significance of the decadal oscillation enhanced and the amplitude increased, with energy spectrum density exceeding the red noise threshold ($p<0.1$). After the 21st century, the significance of the decadal oscillation reached a strong level with high amplitude and intensity, and the primary period has shown a decreasing trend.

4. Analysis of Typhoon Characteristics in the Northwest Pacific

This paper compiles Western North Pacific typhoon data from 1950 to 2024, analyzing typhoon characteristics based on the following four parameters:

- Frequency of typhoons generated in the Western North Pacific per year (referred to as "Typhoon Frequency").
- Average extreme intensity of typhoons generated in the Western North Pacific per year (referred to as "Average Typhoon Intensity").
- Frequency of typhoons making landfall in China per year (referred to as "Landfall Typhoon Frequency").
- Average intensity at the moment of landfall for typhoons hitting China per year (referred to as "Average Landfall Typhoon Intensity").

4.1. Interannual Variation Characteristics

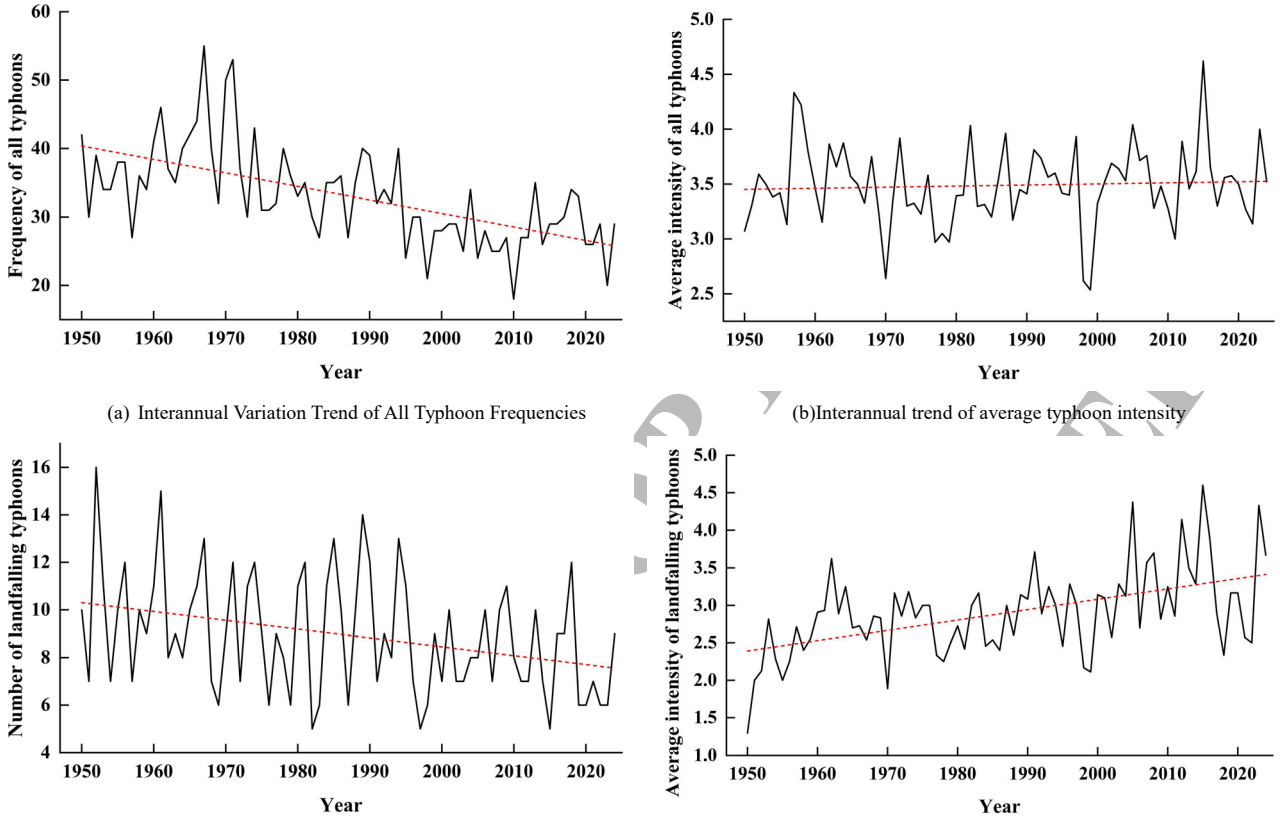

(a) Interannual Variation Trend of All Typhoon Frequencies

(b)Interannual trend of average typhoon intensity

(c) Interannual Trend of Typhoon Landfall Frequency

(d)Interannual trend of average intensity of landfall typhoons

Figure 3: Time Series of Typhoon Characteristics in the Northwest Pacific from 1950 to 2024

Figure 3 shows the time series of Western North Pacific (WNP) typhoon characteristics from 1950 to 2024, including the interannual variation trends of typhoon frequency, average typhoon intensity, landfall typhoon frequency, and average landfall typhoon intensity. According to statistics, between 1950 and 2024, there were a total of 2,482 typhoon activities in the WNP region, averaging approximately 33 per year. A total of 670 typhoons made landfall in China, averaging about 9 per year, with a landfall ratio of approximately 27%. The average intensity of WNP typhoons is approximately 3.49 (Severe Tropical Storm level), while the average intensity of landfall typhoons is approximately 2.90 (Tropical Storm level). The specific interannual variation characteristics of the four sets of typhoon parameters are as follows:

As shown in Figure 3(a), over the 75-year period, the frequency of WNP typhoons shows a significant decreasing trend. According to linear fitting, the typhoon frequency decreased by nearly 15 over these 75 years, a reduction of about 37.5% since 1950. Furthermore, in the 30 years since 1995, the typhoon frequency reached the average level in only 4 years; in nearly 90% of the years, the frequency was below average, and the highest frequency was only 35 in 2013. This indicates a very severe decreasing trend in typhoon frequency. Additionally, the interannual variation of WNP typhoon frequency is large, with a maximum of 55 in 1967 and a minimum of only 20 in 2010.

As shown in Figure 3(b), over the 75-year period, the overall trend of the average intensity of WNP typhoons is not significant, showing a slight increase of nearly 0.1 in the linear fitting results. The interannual variation is large, with the highest intensity of 4.62 (Typhoon level) in 2015 and the lowest intensity of 2.54 (Tropical Storm level) in 1999.

As shown in Figure 3(c), over the 75-year period, the frequency of typhoon landfalls in China also shows a significant decreasing trend. Linear fitting shows a decrease of more than 2 landfalls over the 75 years, a reduction of about 20% since 1950. The interannual variation is substantial, with a maximum of 16 in 1952 and a minimum of 5 in 1982, 1997, and 2015.

As shown in Figure 3(d), over the 75-year period, the average intensity of landfall typhoons shows a significant increasing trend. According to linear fitting, the average intensity of landfall typhoons increased by approximately 1.0, an enhancement of about 41.7% since 1950. The interannual variation is also large, with a maximum intensity of 4.60 (Typhoon level) in 2015 and a minimum of 1.30 (Tropical Depression level) in 1950.

4.2. Characteristics of Changes During the Year

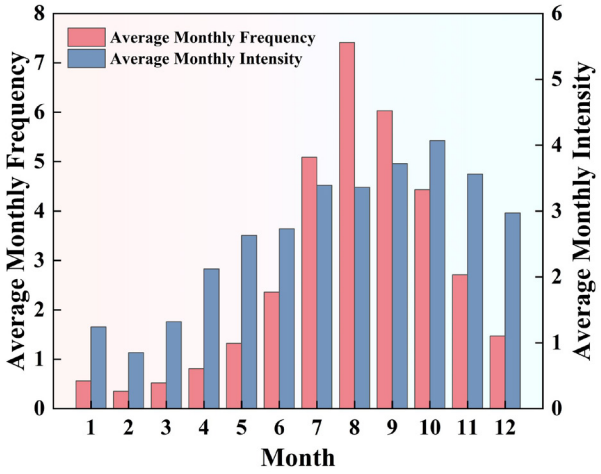

Figure 4: Monthly Average Frequency and Intensity Distribution of Typhoons in the Northwest Pacific from 1950 to 2024

Figure 4 shows the distribution of the average monthly frequency and average intensity of Western North Pacific typhoons from 1950 to 2024, where warm colors represent the average monthly frequency and cool colors represent the average monthly intensity. It can be seen that between 1950 and 2024, there were typhoon activities in every month in the Western North Pacific, and there are obvious variations in typhoon frequency and intensity across different months.

In terms of frequency, August is the month with the most frequent typhoon activity in the Western North Pacific, with an average of 7.41 occurrences; February is the month with the least typhoon activity, with an average of 0.35 occurrences. A frequency below 1 reflects the fact that in many years, no typhoons were generated in February.

In terms of intensity, October is the month with the strongest typhoon activity in the Western North Pacific, with an average intensity of 4.07, reaching the "Typhoon" level on average; February is the month with the weakest typhoon activity, with an average intensity of 0.85, which is below the "Tropical Depression" level on average.

5. Correlation Analysis between ENSO and Typhoons in the Northwest Pacific

5.1. Pearson Correlation Analysis between ENSO and the Interannual Scale of Typhoons in the Northwest Pacific

In exploring the correlation between ENSO and Western North Pacific typhoon activity, this study first employs Pearson correlation analysis for a preliminary assessment. The results of this traditional statistical method serve as a baseline reference, providing a methodological contrast with the subsequent time-frequency localized wavelet analysis. This approach allows for a clearer revelation of coupling characteristics in the relationship between ENSO and typhoon activity that might otherwise be obscured by global correlation.

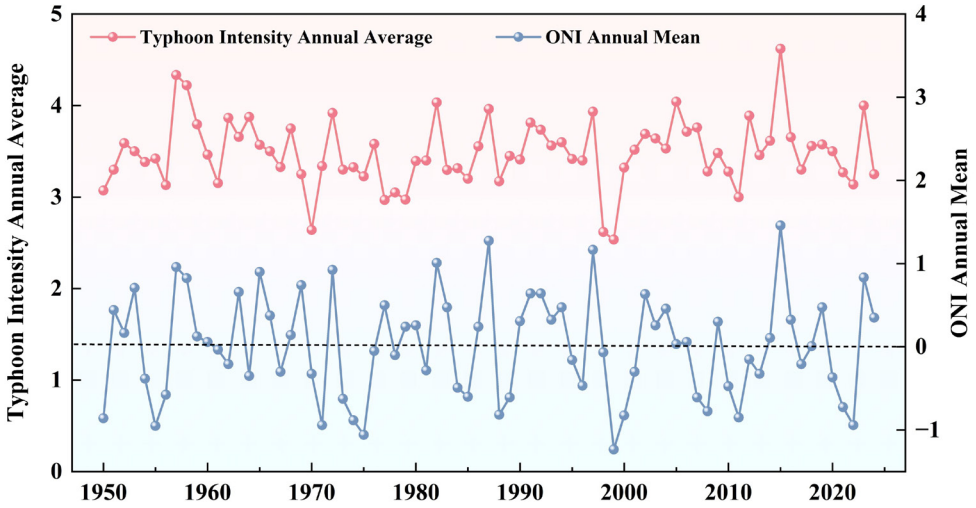

Figure 5: Correlation between ONI and Average Intensity of Typhoons in the Northwest Pacific The Black Dotted Line is the Neutral Position Line of ONI

Since the time scale of the ONI is monthly while the typhoon parameters are annual, in order to conduct a Pearson correlation analysis to preliminarily analyze their association, we first performed an annual arithmetic average of the ONI to obtain an annual average ONI time series (shown as the cool-colored curve in Figure 5). Subsequently, Pearson correlation analysis was conducted between this series and the four sets of typhoon parameter time series, yielding four sets of correlation coefficients, as shown in Table 3. It can be seen that typhoon frequency and landfall typhoon frequency exhibit a negative correlation with the annual average ONI, whereas overall typhoon intensity and landfall typhoon intensity exhibit a positive correlation with the annual average ONI. Among these, overall typhoon intensity shows a strong correlation with the annual average ONI, as illustrated in Figure 5, while the other three show only weak correlations. Table 3 Correlation coefficients between ONI and typhoon in the Northwest Pacific from 1950 to 2024.

Pacific Northwest Typhoon parameters	All typhoons frequency	All typhoons Average strength	Landfall typhoon frequency	Landfall typhoon Average strength
With ONI Correlation Coefficient	-0.112	0.618	-0.298	0.237

5.2. Cross Wavelets and Wavelets Are Correlated with ENSO and Northwest Pacific Typhoons on the Interannual Scale

Continuous Wavelet Transform (CWT) analyzes the time-frequency variation patterns of each variable individually. Based on CWT, Cross Wavelet Transform (XWT) and Wavelet Coherence (WTC) analysis can reveal regions with common signals between the cycles of two variables and their phase relationships [13], providing key tools for exploring the time-frequency correlation between ENSO and Western North Pacific typhoon activity.

In the cross wavelet power spectra and wavelet coherence spectra, the areas enclosed by thick black solid lines represent regions that have passed the 95% red noise confidence test, indicating significant signal zones. The thin solid conical line is the Cone of Influence (COI); regions outside this curve are not considered due to edge effects. The direction of the phase arrows reflects the lead-lag relationship between ENSO and typhoons, allowing for the determination of time delays between the various scale components of the two time series:

- Pointing right (0◦): Indicates the two signals are positively correlated.
- Pointing left (180◦): Indicates the two signals are negatively correlated.
- Pointing up (90◦): Indicates ENSO leads typhoons by 1/4 cycle.
- Pointing down (270◦): Indicates typhoons lead ENSO by 1/4 cycle.
- Pointing upper-right (45◦): Indicates ENSO leads typhoons by approximately 1/8 cycle, with a positive correlation.
- Pointing lower-left (225◦): Indicates typhoons lag behind ENSO by approximately 1/8 cycle, with a negative correlation.

The following are the cross wavelet and wavelet coherence spectra of the four sets of typhoon parameters and the ONI index at the interannual scale, with the left-axis period scale units in years.

5.2.1. ENSO Is Negatively Correlated with Typhoon Frequency

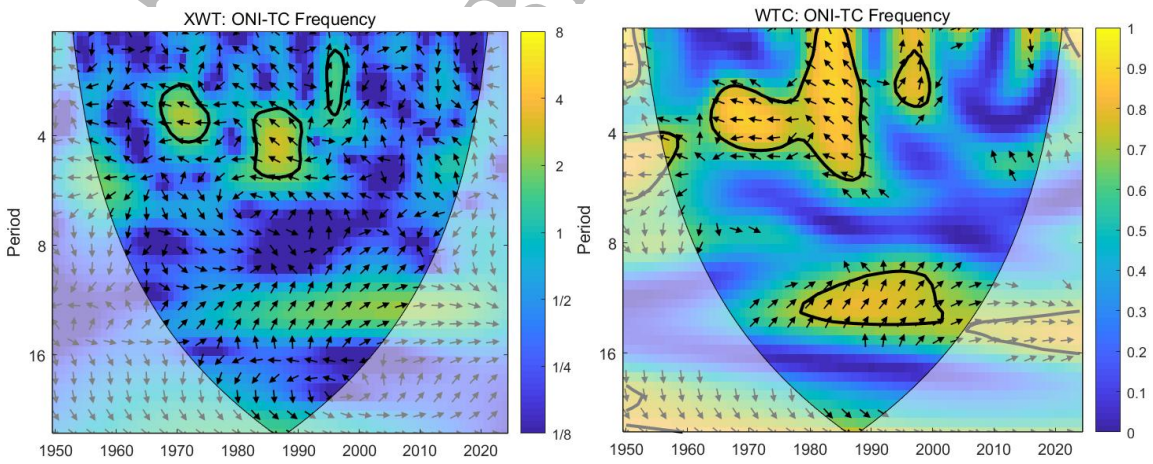

(a)XWT (b) WTC

Figure 6: Cross Wavelet Spectra (XWT) and Wavelet Coherence Spectra (WTC) of Typhoon Frequencies between ONI and the Northwest Pacific from 1950 to 2024 on the Interannual Scale

By comparing Figure 6(a) and (b), it can be observed that within the past 75 years, the cross wavelet spectrum exhibits a significant negative resonance period on the 2–6 year scale and a generally significant positive resonance period on the 10–15 year scale. Both show a strong correspondence in the wavelet coherence spectrum, indicating a significant correlation between ENSO and Western North Pacific typhoon frequency. This correlation possesses time-varying multimodal characteristics, where the positive or negative nature of the correlation varies depending on the chosen period scale—specifically, a negative correlation mode on the 2–6 years scale and a positive correlation mode on the 10–15 years scale. Specifically, from 1960 to 1990, a strong negative correlation existed between ENSO and Western North Pacific typhoon frequency on the 2–6 years cycle; the phase arrows generally point from upper-left to horizontally left, indicating that typhoons slightly led ENSO during this period. Furthermore, the cross wavelet spectrum displays a positive-phase resonance period of 2–4 years between 1995 and 2000, and a positive-phase resonance period of 10–15 years after 1980. This indicates that ENSO and the frequency of all Western North Pacific typhoon activities also showed a significant positive correlation during these intervals, with phase arrows pointing generally toward the upper-right, suggesting that ENSO slightly led typhoons during these times.

5.2.2. ENSO was Significantly Positively Correlated with the Average Intensity of Typhoons

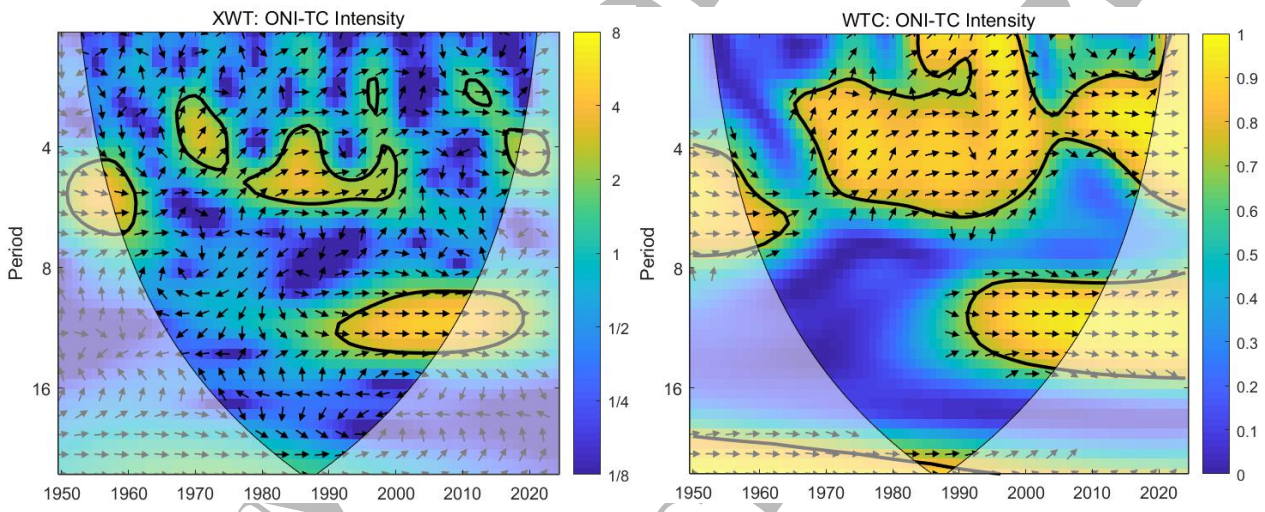

(a) XWT (b) WTC

Figure 7: Cross Wavelet Spectra (XWT) and Wavelet Coherence Spectra (WTC) of ONI and Northwest Pacific Typhoon Intensity at the Interannual Scale from 1950 to 2024

By comparing Figure 7(a) and (b), it can be observed that within the past 75 years, the cross wavelet spectrum exhibits significant positive resonance periods on the 2–6 year and 10–15 year scales, and in the corresponding wavelet coherence spectrum, the significant correlation region on the 2–6 year scale spans almost the entire study period, while the significant correlation region on the 10–15 year scale has also persisted from 1990 to the present, indicating a significant and continuous positive correlation between ENSO and the average intensity of Western North Pacific typhoons on an interannual scale. From 1965 to 1985, the phase arrows on the 2–6 years scale point generally toward the upper-right, indicating that ENSO slightly led typhoons during this period; in other periods, the phase arrows for both the 2–6 year and 10–15 years scales point consistently and horizontally to the right, showing that ENSO and typhoon intensity changed in synchronization.

5.2.3. ENSO Is Negatively Correlated with the Frequency of Landfall Typhoons

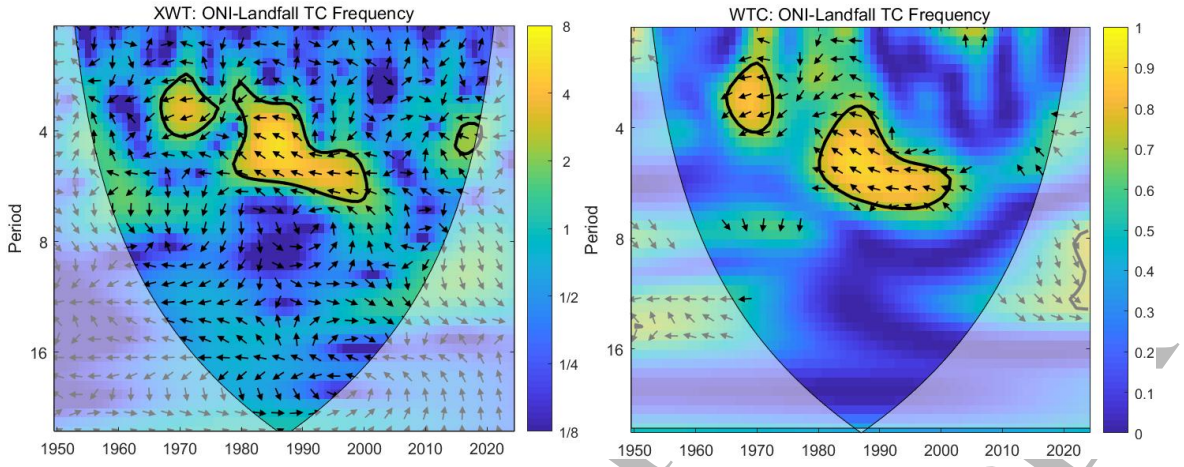

(a) XWT (b) WTC

Figure 8: Cross Wavelet Spectra (XWT) and Wavelet Coherence Spectra (WTC) of the Frequency of ONI and Northwest Pacific Landfall Typhoons from 1950 to 2024 on the Interannual Scale

By comparing Figure 8(a) and (b), it can be observed that within the past 75 years, between 1965 and 2000, the cross wavelet spectrum and the corresponding wavelet coherence spectrum exhibit a significant resonance period on the 2–6 year scale with a negative phase, meaning there is a strong correlation between ENSO and the frequency of Western North Pacific landfall typhoons; the phase arrows generally point from the upper-left to horizontally left, indicating that typhoon variations slightly led ENSO during this period. While the cross wavelet spectrum shows a negative-phase resonance period of 2–6 years between 2015 and 2020, the corresponding correlation on this scale in the wavelet coherence spectrum is not significant; therefore, ENSO and the frequency of Western North Pacific landfall typhoons did not exhibit a clear correlation during that timeframe.

5.2.4. ENSO is Positively Correlated with the Average Intensity of Landfall Typhoons

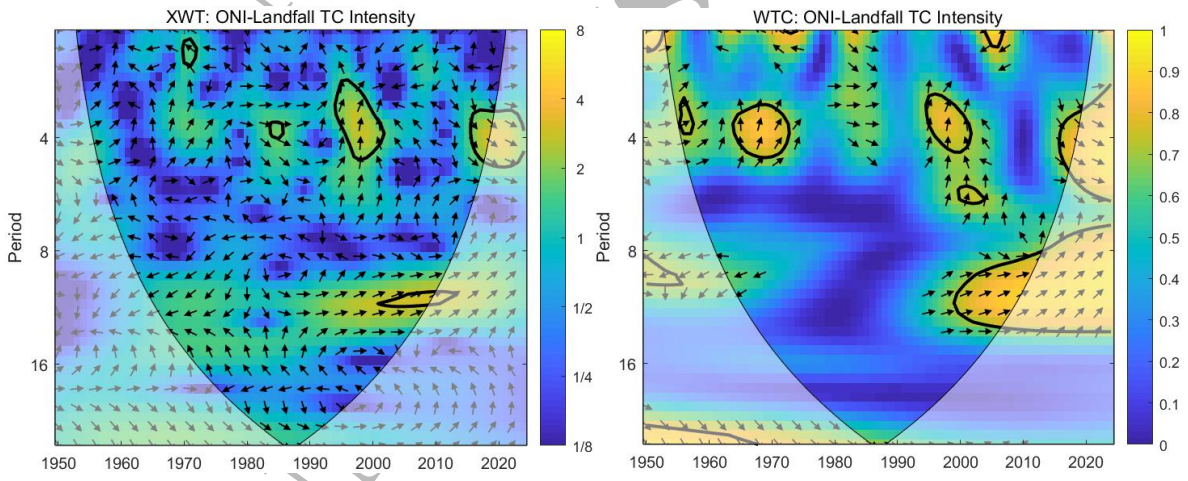

(a) XWT (b) WTC

Figure 9: Interannual ONI and Wavelet Coherence Spectra (WTC) of the Intensity of Landfall Typhoons in the Northwest Pacific from 1950 to 2024

By comparing Figure 9(a) and (b), it can be observed that within the past 75 years, the cross wavelet spectrum exhibits significant positive resonance periods on the 2–6 year and 10–15 year scales; on the corresponding wavelet coherence spectrum, the significant correlation region on the 2–6 years scale persists intermittently throughout the study period, while the significant correlation

region on the 10–15 year scale has persisted from 1995 to the present, indicating a significant and intermittently continuous positive correlation between ENSO and the average intensity of Western North Pacific landfall typhoons on an interannual scale. From 2015 to the present, the phase arrows on the 2–6 years scale point generally from the lower-right to horizontally right, indicating that typhoons slightly led ENSO during this period; in other periods, the phase arrows for both the 2–6 year and 10–15 years scales point basically from horizontally right to vertically upward, with ENSO leading typhoons by up to 1/4 cycle.

Combining the four sets of cross wavelet and wavelet coherence spectra above, we find that only typhoon frequency exhibits time-varying multimodal characteristics. Among the four sets of analyses, ENSO is basically negatively correlated with typhoon frequency and landfall typhoon frequency, while it is positively correlated with average typhoon intensity and average landfall typhoon intensity. Specifically, the correlation between ENSO and average typhoon intensity is the most significant, spanning nearly the entire study period; the correlation with landfall typhoon intensity is relatively significant and persists intermittently throughout the study period; and the correlations with typhoon frequency and landfall typhoon frequency are also relatively significant.

5.3. ENSO and the Interlude Wavelength of Typhoons in the Northwest Pacific Ocean are Coherent with Wavelets

After completing the cross-wavelet and wavelet coherence analysis of ENSO and Western North Pacific typhoons at the interannual scale, this study further focuses on time-frequency correlation characteristics at the monthly scale. The necessity of this approach lies in the fact that the dynamic evolution of ENSO events (such as the developing, mature, and decaying phases) and their modulating effects on typhoon activity often exhibit significant phase-dependent differences; interannual analysis may obscure the details of such short-period interactions. Through monthly-scale wavelet analysis, it is possible to more precisely capture the time-varying coupling relationship between ENSO signals and typhoon frequency and intensity.

Since the time scale of the ONI is monthly while the typhoon parameters are annual, to further analyze their correlation at the monthly scale, we first converted the typhoon parameters into monthly anomaly data to obtain monthly anomaly time series. These were then used for cross-wavelet and wavelet coherence analysis with the ONI time series. Considering that landfall typhoons only occur during the summer and autumn, and their frequency/intensity is essentially zero during winter and spring—lacking global continuity—the monthly scale analysis only discusses typhoon frequency and overall typhoon intensity. The following are the cross-wavelet and wavelet coherence spectra of typhoon frequency, overall average typhoon intensity, and the ONI index at the monthly scale, with the left-axis period scale units in months.

5.3.1. At the Monthly Scale, ENSO was Significantly Negatively Correlated with Typhoon Frequency

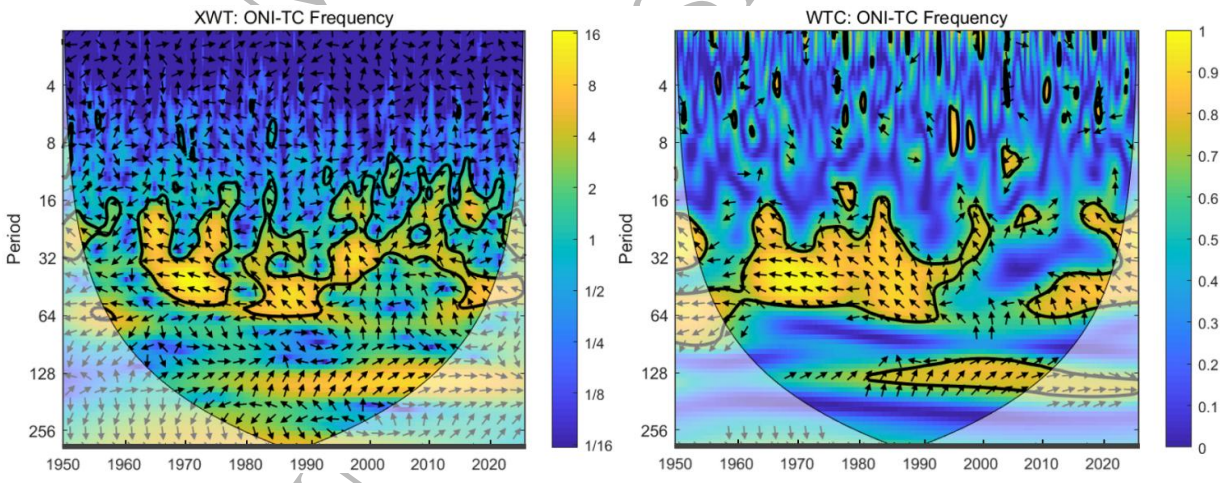

(a) XWT (b) WTC

Figure 10: Cross Wavelet Spectra (XWT) and Wavelet Coherence Spectra (WTC) of the Anomaly between ONI and Northwest Pacific Typhoon Frequencies at the Intermonthly Scale from 1950 to 2024

By comparing Figure 10(a) and (b), it can be observed that within the past 75 years, the cross wavelet spectrum exhibits a significant negative resonance period near the 2–6 year scale, which spans almost the entire study period; additionally, a generally significant positive resonance period exists near the 10–15 year scale. In the corresponding wavelet coherence spectrum, the significant correlation region on the 2–6 years scale persists throughout nearly the entire study period, while the significant correlation region on

the 10–15 years scale has persisted from 1995 to the present. This indicates that at the monthly scale, a significant correlation exists between ENSO and Western North Pacific typhoon frequency, and this correlation also exhibits time-varying multimodal characteristics—specifically, a negative correlation mode on the 2–6 years scale and a positive correlation on the 10–15 years scale. At the monthly scale, ENSO and Western North Pacific typhoon frequency show a significant negative correlation on the 2–6 years scale, with phase arrows generally pointing from the upper-left to horizontally left, indicating that typhoons slightly led ENSO during this period; furthermore, they show a significant positive correlation on the 10–15 year scale, with phase arrows pointing generally from the upper-right to horizontally right, indicating that ENSO slightly led typhoons during this timeframe.

5.3.2. At the Intermonthly Scale, ENSO was Significantly Positively Correlated with the Average Intensity of Typhoons

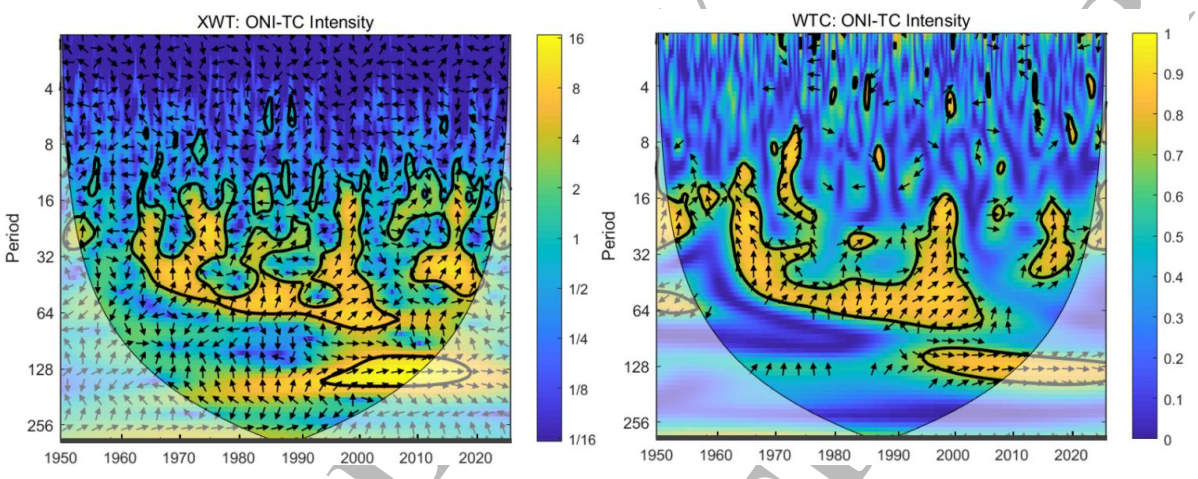

(a) XWT (b) WTC

Figure 11: Cross Wavelet Spectra (XWT) and Wavelet Coherence Spectra (WTC) of Anomalies between ONI and all Typhoons in the Northwest Pacific at the Intermonthly Scale from 1950 to 2024

By comparing Figure 11(a) and (b), it can be observed that within the past 75 years, the cross wavelet spectrum exhibits significant positive resonance periods on the 2–6 year and 10–15 year scales; in the corresponding wavelet coherence spectrum, the significant correlation region on the 2–6 year scale persists intermittently throughout the study period, while the significant correlation region on the 10–15 year scale has persisted from around 1995 to the present, indicating a significant and intermittently continuous positive correlation between ENSO and the average intensity of Western North Pacific typhoons at the monthly scale. From 1960 to 1970, a brief negative correlation appeared on the 2–6 years scale, with phase arrows pointing generally from vertically upward to the upper-left, indicating that typhoons slightly led ENSO during this period; in other periods, the phase arrows for both the 2–6 year and 10–15 years scales point generally from horizontally right to vertically upward, indicating that ENSO led typhoons and the two were positively correlated.

Combining the two sets of cross wavelet and wavelet coherence spectra above, we find that at the monthly scale, the correlation between ENSO and typhoon frequency is more significant than at the interannual scale, with the correlation spanning nearly the entire study period; however, the correlation between ENSO and average typhoon intensity is less significant than at the interannual scale, with the correlation persisting intermittently throughout the study period. The positive and negative correlations between ENSO and typhoon frequency still exhibit different directional characteristics depending on the chosen period scale.

6. Conclusion and Discussion

6.1. Conclusion

Based on the Ocean Niño Index (ONI) and Western North Pacific typhoon data from 1950–2024, this study analyzed the intensity variations and time-frequency characteristics of ENSO, examined the characteristic changes in Western North Pacific typhoon frequency, average typhoon intensity, landfall typhoon frequency, and landfall typhoon intensity, and finally analyzed the correlation between ENSO and Western North Pacific typhoon activity. The main conclusions are as follows:

- Between 1950–2024, a total of 24 El Niño events and 20 La Niña events occurred. El Niño events occurred more frequently and had a higher average peak intensity than La Niña events, while La Niña events had a longer average duration than El Niño events.
- Between 1950–2024, ENSO exhibited multi-scale periodic variations. In the frequency domain, there was an interannual oscillation with a time scale of 94 months (approx. 7–8 years) and a temporal period of about 5 years; there was also a decadal oscillation with a time scale of 198 months (approx. 16–17 years) and a temporal period of about 10–11 years.

- Between 1950–2024, the Western North Pacific region recorded a total of 2,482 typhoon activities, averaging about 33 per year with an average intensity of 3.49 (Severe Tropical Storm level). A total of 670 typhoons made landfall in China, averaging about 9 per year with an average intensity of 2.90 (Tropical Storm level). Regarding interannual trends, Western North Pacific typhoon frequency and landfall frequency decreased significantly, while landfall intensity increased significantly. Seasonally, Western North Pacific typhoons are most frequent in August and least frequent in February; intensity is strongest in October and weakest in February.
- Cross-wavelet transform and wavelet coherence analysis indicate that ENSO is negatively correlated with typhoon frequency and landfall typhoon frequency on a 2–6 years scale with moderate significance, suggesting that ENSO has a certain inhibitory effect on Western North Pacific typhoon frequency, with typhoon activity slightly leading ENSO. ENSO is positively correlated with average typhoon intensity and average landfall typhoon intensity on the 2–6 year and 10–15 years scales with strong significance, indicating that ENSO significantly enhances Western North Pacific typhoon intensity, with ENSO activity slightly leading the typhoons.
- At the monthly scale, the correlation between ENSO and typhoon frequency is more significant than at the interannual scale, whereas the correlation between ENSO and average typhoon intensity is less significant than at the interannual scale. Furthermore, the positive and negative correlations between ENSO and typhoon frequency exhibit different directions depending on the chosen period scale.

6.2. Discussion

The regulatory mechanisms of ENSO on Western North Pacific typhoon frequency and intensity are complex. The mechanisms by which ENSO inhibits frequency while enhancing intensity can be analyzed from several perspectives: During El Niño, the abnormal warming of the equatorial Eastern Pacific triggers anomalies in the Walker circulation, strengthening descending motion in the Western North Pacific and suppressing convection. Simultaneously, the weakening of the southeast trade winds causes warm pool water to flow eastward, leading to a decrease in sea surface temperatures (SST) in the Western North Pacific warm pool. These disrupted formation conditions suppress typhoon frequency. Furthermore, the drop in SST causes the Subtropical High to retreat eastward, shifting the monsoon trough eastward and southward. This forces typhoon formation zones to shift toward the open ocean. Typhoons generated in these distant waters have longer migration paths and stay longer over open sea, providing them with more time to absorb oceanic heat. Additionally, under the context of global warming, the overall rise in Western North Pacific SST provides extra energy for intensification despite fewer total occurrences, thus enhancing typhoon intensity [35-38].

The fact that the negative correlation with typhoon frequency is more significant at the monthly scale, while the positive correlation with intensity is more prominent at the interannual scale, deepens our understanding of the spatio-temporal differentiation of ENSO's regulation. This complements the research regarding the enhancement of summer typhoon activity by persistent La Niña events; while the latter emphasizes the impact of ENSO duration, this study resolves the dynamic association from the perspective of periodic characteristics [39].

When ENSO enhances Western North Pacific typhoon intensity, the ENSO variation leads the typhoon variation. This conclusion supports the theory that ENSO indirectly affects typhoon intensity by modulating large-scale environmental fields. It echoes the research by Huang et al. On the irreversibility of the Western North Pacific anomalous anticyclone, which points out that ENSO influences atmospheric circulation by regulating SST anomalies; meanwhile, this study reveals the phase-lead relationship of ENSO over typhoon changes through wavelet analysis [40,41,24].

Despite the progress made, several limitations remain: 1) Insufficient ENSO classification: The current analysis does not distinguish between Eastern Pacific (EP) and Central Pacific (CP) El Niño/La Niña events. CP El Niño events may alter intensity distributions by extending the duration of rapid intensification, a heterogeneity that this study may have obscured. Future research could construct a dynamic ENSO classification framework to quantify response differences. 2) Limitations in mechanistic explanation: This study is primarily based on statistical correlation and lacks quantitative analysis of physical processes (e.g., air-sea interaction, latent heat flux changes). Subsequent research could utilize CESM or CMIP6 models to conduct air-sea coupling experiments to quantify the relative contributions of ocean heat content and vertical wind shear. 3) Data resolution constraints: Reliance on historical meteorological records may lead to an underestimation of early typhoon intensities. Future work could incorporate satellite remote sensing inversion data (e.g., SST and wind field reconstruction) to improve accuracy [42].

References

1. Zhou, S., Zhang, R. Y., & Zhang, C. (1997). Meteorology and climatology. *China Higher Education Press: Beijing, China*, 2-15.
2. Gao, J., Zhu, X., Yu, Y., & Jin, B. (1999). Study of the impact of typhoon disaster on coastal region of China. *J. Catastrophol, 14*, 73-7.
3. Jiangnan, L., Zhipeng, G., Anyu, W., et al. (2004). Tropical Geography. 02, 113-117.
4. Liang, B., Liang, J., & Wen, Z. (1995). Study of Typhoon Disasters and Its Effects in China. In *Chinese Science Abstracts Series B* (Vol. 3, No. 14, pp. 69-70).
5. Lianshou, C., & Zhiyong, M. (2001). Ten Years of Research on Tropical Cyclones in our country. *Atmospheric Science* 03, 420-432.
6. Zhang, W., Tao, W., Huang, G., Hu, K., Qu, X., Gong, H., ... & Wang, Y. (2024). Irreversibility of ENSO impacts on the wintertime anomalous Western North Pacific anticyclone to CO2 forcing. *npj Climate and Atmospheric Science, 7*(1), 299.
7. Aifang, S., Xiaona, L., & Liman, C., et al. (2021). Basic observation and analysis of extreme rainstorm weather in

Zhengzhou "7.20". *Rainstorm Disaster, 40*(05), 445-454.
8. Chaolu, B., Anran, Z., & Zuowei, X., et al. (2022). "7.20" Henan rainstorm water vapor transport characteristics and its key weather scale system. *Atmospheric Science,46*(03), 725-744.
9. Zheng, L., Lanlan, Q., Wei, W., Bin, H., Shaohong, W., & Shanfeng, H. (2024). Spacio-Temporal Variation Characteristics of Northward-Moving Typhoon and Their Relationship with ENSO. *Tropical Geography, 44*(6).
10. Mengxue, C., Chunyi, X., & Hanyun, Z., et al. (2023). Characteristics analysis of extreme heavy precipitation caused by Typhoon "Dusuri" (2305). *Journal of Marine Meteorology, 43*(04), 11-20.
11. Chongyin, L. (2002). Climate and Environment Research, (02), 160-174.
12. Shaowu, W., & Daoyi, G. (1999). ENSO events and their intensity in the past 100 years. Meteorology, (01), 10-14.
13. Fan, F., Lin, R., Fang, X., Xue, F., Zheng, F., & Zhu, J. (2021). Influence of the eastern Pacific and central Pacific types of ENSO on the South Asian summer monsoon. *Advances in Atmospheric Sciences, 38*(1), 12-28.
14. Huangfu, J., Huang, R., Chen, W., & Feng, T. (2018). Causes of the active typhoon season in 2016 following a strong El Niño with a comparison to 1998. *International Journal of Climatology, 38*, e1107-e1118.
15. Li, S., Li, Z., & Ling, S. (2023). Combined effect of the solar activity and ENSO on the tropical cyclone genesis frequency in the southeastern part of the western North Pacific. *Frontiers in Earth Science, 11*, 1139699.
16. Huang, F., & Xu, S. (2010). Super typhoon activity over the western North Pacific and its relationship with ENSO. *Journal of Ocean University of China, 9*(2), 123-128.
17. Kang, N. Y., Kim, D., & Elsner, J. B. (2019). The contribution of super typhoons to tropical cyclone activity in response to ENSO. *Scientific reports, 9*(1), 5046.
18. Yong, H., Chongyin, L., & Ying, W., et al. (2008). Relationship between the frequency of tropical cyclones in the northwest Pacific Ocean and ENSO in the past 100 years[J]. Ocean Forecast (01), 80-87.
19. 桂辛未, 李自强, 张水平, 孟昭祎, 高淑敏, 王士成, & 宗. (2023). 西北太平洋厄尔尼诺年与拉尼娜年的热带气旋路径对比. 海洋湖沼通报, 1-7.
20. Yali, X., & Xiajiang. H. (1998). Influence of El Niño event on tropical cyclone activity. Guangdong Meteorology (03), 22-23.
21. Lanhua, M., Xuan, C., & Shaoyan, H., et al. (2018). Impact of ENSO events on landfall in tropical cyclones in China from 1951 to 2016. *Soil and Water Conservation Research,25*(05), 325-329+336.
22. Qianqian, J., Feng, X., & Yu, Z. (2018). *Journal of Guangdong Ocean University,38*(02), 71-79.
23. Qianqian, Y., Dongmei, X., & Yongping, C., et al. (2022). A preliminary study on the relationship between tropical cyclones affecting the coast of China and ENSO changes from 1979 to 2019. *Ocean Bulletin, 41*(01), 29-38.
24. Yu-Meng, L., Rui-Fen, Z., & Yi-Hui, D. (2025). Multi-Scale Influencing Factors and Prediction of Interannual Variability in Rapid Intensification Magnitude of Northwest Pacific Tropical Cyclones. *Journal of Tropical Meteorology, 31*(1), 75-86.
25. Trenberth, K. E. (1997). The definition of el nino. *Bulletin of the American Meteorological Society, 78*(12), 2771-2778.
26. Trenberth, K. E., & Stepaniak, D. P. (2001). Indices of el Niño evolution. *Journal of climate, 14*(8), 1697-1701.
27. Ying, M., Zhang, W., Yu, H., Lu, X., Feng, J., Fan, Y., ... & Chen, D. (2014). An overview of the China Meteorological Administration tropical cyclone database. *Journal of Atmospheric and Oceanic Technology, 31*(2), 287-301.
28. Lu, X., Yu, H., Ying, M., Zhao, B., Zhang, S., Lin, L., ... & Wan, R. (2021). Western North Pacific tropical cyclone database created by the China Meteorological Administration. *Advances in Atmospheric Sciences, 38*(4), 690-699.
29. China Meteorological Administration. 2006. Tropical cyclone classification standard: GB/T19021-2006. Beijing: China Standard Press.
30. Huang, B., Thorne, P. W., Banzon, V. F., Boyer, T., Chepurin, G., Lawrimore, J. H., ... & Zhang, H. M. (2017). Extended reconstructed sea surface temperature, version 5 (ERSSTv5): upgrades, validations, and intercomparisons. *Journal of climate, 30*(20), 8179-8205.
31. Ren, H. L., Lu, B., Wan, J., Tian, B., & Zhang, P. (2018). Identification standard for ENSO events and its application to climate monitoring and prediction in China. *Journal of Meteorological Research, 32*(6), 923-936.
32. Zhao, Z. C., Luo, Y., & Huang, J. B. (2023). Global warming and El Niño events. *Climate Change Research, 19*(5), 663-666.
33. 虹颖, 徐峰, 李晓惠, 夏天竹, & 张羽. (2017). 近 65 年 ENSO 事件强度变化及时频特征研究. 气象学报, 33(5), 683-694.
34. Yang, X., Xuguang, S., & Yan, Y., et al. (2017). Changes in ENSO characteristics under the background of global warming. *Science Bulletin, 62*(16) 1738-1751.
35. Guo, Y. P., & Tan, Z. M. (2018). Westward migration of tropical cyclone rapid-intensification over the Northwestern Pacific during short duration El Niño. *Nature Communications, 9*(1), 1507.
36. Guo, Y. P., & Tan, Z. M. (2021). Influence of different ENSO types on tropical cyclone rapid intensification over the western North Pacific. *Journal of Geophysical Research: Atmospheres, 126*(11), e2020JD033059.
37. Yu, J. H., Ou, L., Chen, L., Li, L., Sun, M., Zhong, X., & Zhang, X. (2021). Tropical cyclone genesis over the western North Pacific impacted by SST anomalies from other basins while El Niño decays. *Quarterly Journal of the Royal Meteorological Society, 147*(737), 2580-2596.
38. Jian, D., Zhao, H., Klotzbach, P. J., Raga, G. B., Gao, J., Cao, J., ... & Ma, Z. (2024). Projected poleward migration of western North Pacific tropical cyclone genesis. *Geophysical Research Letters, 51*(16), e2024GL110031.
39. Luo, X., Yang, L., Chan, J. C., Chen, S., Peng, Q., & Wang, D. (2024). China coasts facing more tropical cyclone risks

during the second decaying summer of double-year La Niña events. *npj Climate and Atmospheric Science, 7*(1), 198.
40. Peng, Z., Yunxia, Z., Yang, W., Yi, D., Yizhou, Y., Zhen, D., & Xihong, W. (2024). Analysis of Temporal-Spatial Patterns and Impact Factors of Typhoon Disaster Losses in China from 1978 to 2020. *Tropical Geography, 44*(6).
41. Jing-xian, Z., Xiao-yu, C., & Hua-dong, Y. (2025). Evolving Characteristics and Intensified Influences of Landfalling Tropical Cyclones in East China During 1965–2022. *Journal of Tropical Meteorology, 31*(5), 511-518.
42. Da, L., Chunyi, X., & Ling, Z., et al. (2023). Analysis of the main characteristics of typhoon "Dusuri" (2305) and the difficulties in forecasting its path and intensity. *Journal of Marine Meteorology 43*(04), 1-10.